Effect of coating density on oxidation resistance and Cr vaporization from solid oxide fuel cell interconnects

Talic, Belma; Falk-Windisch, Hannes; Venkatachalam, Vinothini; Hendriksen, Peter Vang; Wiik, Kjell; Lein, Hilde Lea

Published in:
Journal of Power Sources

Link to article, DOI:
10.1016/j.jpowsour.2017.04.023

Publication date:
2017

Document Version
Peer reviewed version

Effect of coating density on oxidation resistance and Cr vaporization from solid oxide fuel cell interconnects

Belma Talic[a,c] (beltal@dtu.dk, +45 61 41 84 52)*,

Hannes Falk-Windisch[b] (hannes.windisch@chalmers.se),

Vinothini Venkatachalam[c] (viven@dtu.dk),

Peter Vang Hendriksen[c] (pvhe@dtu.dk),

Kjell Wiik[a] (kjell.wiik@ntnu.no),

Hilde Lea Lein[a] (hilde.lea.lein@ntnu.no)

[a]Department of Materials Science and Engineering, Norwegian University of Science and Technology, Sem Sælands Vei 12, 7491 Trondheim, Norway

[b]Department of Chemistry and Chemical Engineering, Division of Energy and Materials, Chalmers University of Technology, Kemivägen 10, SE-41296 Gothenburg, Sweden

[c]Department of Energy Conversion and Storage, Technical University of Denmark, DTU Risø Campus, Frederiksborgvej 399, DK-4000 Roskilde, Denmark

*Corresponding author

Abstract. Manganese cobalt spinel oxides are promising materials for protective coatings for solid oxide fuel cell (SOFC) interconnects. To achieve high density such coatings are often sintered in a two-step procedure, involving heat treatment first in reducing and then in oxidizing atmospheres. Sintering the coating inside the SOFC stack during heating would reduce production costs, but may

result in a lower coating density. The importance of coating density is here assessed by characterization of the oxidation kinetics and Cr evaporation of Crofer 22 APU with $MnCo_{1.7}Fe_{0.3}O_4$ spinel coatings of different density. The coating density is shown to have minor influence on the long-term oxidation behavior in air at 800 °C, evaluated over 5000 h. Sintering the spinel coating in air at 900 °C, equivalent to an *in-situ* heat treatment, leads to an 88 % reduction of the Cr evaporation rate of Crofer 22 APU in air-3% H_2O at 800 °C. The air sintered spinel coating is initially highly porous, however, densifies with time in interaction with the alloy. A two-step reduction and re-oxidation heat treatment results in a denser coating, which reduces Cr evaporation by 97 %.

Keywords: Solid Oxide Fuel Cell, Metallic Interconnect, Manganese Cobalt Spinel, Ceramic Coating, High Temperature Oxidation, Chromium Evaporation

1. Introduction

As the operating temperature of Solid Oxide Fuel Cells (SOFC) has been reduced over the last decades, ferritic stainless steels (FSS) have become the preferred choice for the interconnect material [1]. FSS offer several advantages over the previously used $LaCrO_3$-based ceramic interconnect such as lower costs, higher electrical and thermal conductivities, and a much easier manufacturing process [2,3]. Nevertheless, the use of FSS as the interconnect materials poses challenges. Under SOFC operating conditions, the steel oxidizes to form a scale consisting of Cr_2O_3 and $(Mn,Cr)_3O_4$ that grows with time. Because of the modest electrical conductivity of these oxides, the stack resistance increases [4]. Furthermore, the oxide scale in reaction with oxygen and water vapor forms volatile Cr(VI)-species that have been reported to “poison” the SOFC cathode [5,6]. There have been some attempts to develop new cathode materials with higher Cr tolerance [7–9]. However, this does not eliminate the problem of high Cr evaporation rates as Cr depletion from the alloy below a certain limit may lead to break-away type oxidation [10,11]. Cr evaporation has a low activation energy and will therefore continue to be a challenge even if the operating temperature of SOFC is further reduced [12].

$(Mn,Co)_3O_4$ spinels are promising coating materials for reducing scale growth and Cr evaporation from FSS [13–18]. Several methods to deposit these coatings are under consideration, including various slurry spraying methods [19–21], screen printing [22], electrophoretic deposition (EPD) [23,24], electroplating [25] and atmospheric plasma spraying [26,27]. EPD is particularly promising as it is a fast and cheap method that offers good control of layer thickness and the opportunity to coat geometrically complex structures [28]. A common denominator for all powder-based methods such as EPD is the necessity to sinter the coating after deposition. To ensure a high coating density while attempting to avoid excessive oxidation of the steel, a two-step procedure has been employed for sintering of spinel coatings [15,22]. The first step is heat treatment in N_2+H_2 (or equivalent reducing atmosphere) where the spinel oxide decomposes into MnO and Co [29]. The second step is heat treatment in air where the spinel phase is re-formed and densification is promoted by a reaction-sintering type mechanism [30,31]. The two-step sintering procedure has in some assessments been estimated to make up approximately 20 % of the total interconnect coating costs [32,33]. From a commercial point-of-view, it would therefore be beneficial if the coating instead could be densified inside of the SOFC stack during initial warm-up. However, very little densification of $(Mn,Co)_3O_4$ is achieved in air at moderate temperatures. Dilatometry measurements by Lee et al. [22] showed that the linear shrinkage of $Mn_{1.5}Co_{1.5}O_4$ in air is less than 3 % below 1000 °C.

Only few studies have investigated how the $(Mn,Co)_3O_4$ spinel coating density affects Cr evaporation and oxidation behavior of FSS. Kurokawa et al. [13] measured the Cr vaporization rate of $MnCo_2O_4$ coated SS430, where differences in powder manufacturing methods lead to two different levels of coating density. After 24 h of exposure at 800 °C, the Cr vaporization rate was reduced by a factor of three with a porous coating, while a denser coating reduced the Cr vaporization rate by a factor of 40 [13]. Akanda et al. [33] compared the ASR of SS441 with a $(Mn,Co)_3O_4$ coating sintered either in air or by the two-step reduction and re-oxidation procedure. They concluded that a highly dense coating, achieved by the two-step procedure, was necessary to avoid excessive scale growth leading to

unacceptably high ASR. The conclusion was based on accelerated testing at 900 °C, while the initial measurement at 800 °C for 1000 h indicated a low and stable ASR also for the sample with a highly porous coating. Molin et al. [18] evaluated the ASR of $MnCo_2O_4$ and $MnCo_{1.8}Fe_{0.2}O_4$ coated Crofer 22 APU over 5000 h at 750 °C. The oxide powders were brush painted on the steel to create a porous matrix, which was impregnated with an ethanol based solution of Mn, Co and Fe nitrates containing ethylene glycol and citric acid. The impregnation was expected to improve sinterability and the coatings were not sintered before the ASR measurement. Coated samples resulted in a four times slower linear increase in ASR compared to uncoated Crofer 22 APU. Post-mortem analysis showed that the initially very porous coatings had densified near the thermally grown oxide interface.

Thus, there are indications in literature that even highly porous spinel coatings may provide protection of FSS interconnects. However, there is a shortage of long term studies at realistic SOFC operating temperatures where the effect of coating density is evaluated.

In this work, we have investigated long term (5000 h) oxidation behavior of Crofer 22 APU with $MnCo_{1.7}Fe_{0.3}O_4$ coatings heat treated to produce different levels of coating density. In addition, Cr evaporation from Crofer 22 APU with coatings of different density has been measured during 500 h exposure to humidified air. $MnCo_{1.7}Fe_{0.3}O_4$ was chosen as the coating because the thermal expansion coefficient (TEC) of this material between room temperature and 800 °C (12.0×10^{-6} K^{-1}) is lower than that of $MnCo_2O_4$ (14.4×10^{-6} K^{-1}) [34]. The lower value provides a better match to the TEC of Crofer 22 APU (11.9×10^{-6} K^{-1}, 20-800 °C [35]), which reduces build-up of stresses during thermal cycling and consequently the risk of coating spallation.

2. Experimental

A plate of 1 mm thick Crofer 22 APU (Thyssen Krupp) with the composition given in Table 1 was cut into coupons of 20×20 mm. A 3 mm hole was drilled in one of the corners to allow for hanging in the

oxidation furnace. The coupons were ground with SiC-paper, polished down to 1 μm using diamond abrasive and cleaned in acetone and ethanol for 10 minutes each in an ultrasonic bath. Sample thickness measured after grinding was typically 0.8-0.9 mm.

Table 1. Composition of Crofer 22 APU alloy used in this study in wt.%. Analyzed by Optical Emission Spectroscopy (OES) at Force Technology, Denmark.

Alloy	Fe	Cr	Mn	Ti	La	C	Si	Al
Crofer 22 APU	Bal.	23	0.42	0.068	0.04-0.20[1]	0.003	0.049[2]	0.007

[1]La was not analyzed by OES. Concentration according to the manufacturer's datasheet

[2]Determination of Si content by OES is associated with large uncertainty

The steel coupons were coated by electrophoretic deposition (EPD). $MnCo_{1.7}Fe_{0.3}O_4$ spinel powder was synthesized by spray pyrolysis of an aqueous based nitrate solution as described in [34]. The powder was calcined at 650 °C for 5 h, ball milled overnight in 100 % ethanol (250 ml PE-bottle, Ø 10 mm YSZ milling balls), and dried in a rotary evaporator before use. The particle size distribution of the powder after milling was bimodal with a median size (d_{50}) equal to 0.63 μm. A suspension for EPD was prepared by ball milling 5 wt.% spinel powder in a 50/50 vol.% mixture of ethanol and isopropanol for 48 h (500 ml PE-bottle, Ø 10 mm YSZ milling balls). Two ca. 50×50 mm plates of Crofer 22 APU were used as counter electrodes during deposition. The sample was placed in parallel between these two plates at a distance of 15 mm. A constant voltage of 35 V was applied for 90 s with the negative terminal connected to the sample, resulting in a deposit of approximately 7.6 mg cm^{-2} of powder. A small area of the sample (~ 1 %) was left uncoated due to coverage by the electrode clip during EPD.

After drying in air at room temperature, the samples were heat treated following one of the three procedures described in Table 2. The heating and cooling rates were 120 °C h^{-1}. Gases were bubbled

through water at 5 °C to give a moisture content of ca. 1 %. Uncoated Crofer 22 APU was heat treated under the same conditions to estimate mass change due to oxidation of the alloy during coating sintering. Surface structural characterization of coated samples after sintering was performed on a Bruker D8 X-ray diffractometer (XRD) with Cu Kα radiation. The diffractograms were collected on rotating samples from 15-75° 2θ using a step size of 0.02° and a collection time of 1 s per step.

Table 2. Heat treatment procedures for sintering $MnCo_{1.7}Fe_{0.3}O_4$ spinel coating on Crofer 22 APU and abbreviations for each method, used throughout the text.

Abbreviation	1: Reduction step (R)	2: Oxidation step (O)
O900		2 h at 900 °C in air
R900+O800	2 h at 900 °C in N_2-9%H_2	2 h at 800 °C in air
R1100+O800	5 h at 1100 °C in N_2-9%H_2	5 h at 800 °C in air

The oxidation behavior of coated samples was evaluated over 5000 h in air at 800 °C in a chamber furnace. There was no forced air flow to the furnace (i.e. nearly stagnant conditions) and the humidity content was not controlled. Polished Crofer 22 APU without any coating was oxidized under the same conditions for 2000 h. At least three samples of each type were suspended vertically in the furnace (hanging from an alumina rod). Every 250 h, the furnace was cooled to room temperature (180 °C h^{-1}) and the samples were weight on a scale with 0.00001 g accuracy (XS205 Mettler Toledo). One sample of each type was taken out after 2000 h and 5000 h of oxidation for inspection by scanning electron microscopy (SEM, Zeiss Supra 35 field emission-SEM and Zeiss Merlin field emission-SEM) and energy dispersive X-ray spectroscopy (EDX, Bruker X-Flash 6160). The EDX data were collected at an acceleration voltage of 15 kV and analyzed using Esprit software (Bruker). Quantification (standardless) was performed using only the Kα lines for Cr, Mn, Co and Fe.

Additional samples were oxidized in flowing air with 3 % H_2O while measuring chromium evaporation by the Denuder method. The method is described in detail in [36], and estimated to have a 95±5 % collection efficiency. The targeted moisture content was ensured by passing cleaned, dry air through a membrane (Perma Pure FC-Series humidifier) connected to a water bath at 24.4 °C. The flow rate of the gas was set to 6000 ml min^{-1}. A porous Al_2O_3 flow restrictor was placed in front of the samples to ensure a uniform flow pattern. A quartz tube (6 mm inner diameter) coated with Na_2CO_3 was placed behind the samples to "catch" Cr-species in the gas outlet. Volatile Cr species from the sample react with the carbonate to form chromate according to reaction (1):

$$CrO_2(OH)_2(g) + Na_2CO_3(s) \rightarrow Na_2CrO_4(s) + H_2O(g) + CO_2(g) \quad (1)$$

The quartz tubes were exchanged approximately every 100 h and rinsed with distilled water to dissolve the sodium chromate. The amount of chromate in the solution was quantified by spectrophotometry (Evolution 60S, Thermo Scientific).

For the O900 samples, Cr evaporation was measured during sintering to obtain a measure for the total Cr evaporation if the coating is sintered inside of the SOFC stack during warm-up (i.e. *in-situ*). For this purpose, coated samples were placed in the furnace at 150 °C, heated to 900 °C for 2 h and cooled to 500 °C before exchanging the quartz tube. Cr evaporation during the R1100+O800 reduction and re-oxidation heat treatment was not measured since this type of sintering would be performed before the interconnect is placed in the SOFC stack (i.e. *ex-situ*).

Subsequent exposure of the O900 samples, those sintered ex-situ (R1100+O800) and uncoated Crofer 22 APU was made by placing samples in the furnace at 300 °C and heating to 800 °C (heating rate 240 °C h^{-1}). The exposure was continuous for 500 h. All measurements were performed in two

different furnaces under identical conditions to check for reproducibility. The total surface area of samples in each test was 15.7 cm^2. The sample cross sections were examined by SEM after exposure.

3. Results

3.1 Microstructure after coating preparation

SEM cross sections of $MnCo_{1.7}Fe_{0.3}O_4$ coated Crofer 22 APU after the three different sintering heat treatments are shown in Figure 1a)-c). The coating thickness varies among samples by around 5 μm. The alloy is oxidized to varying degree during the different sintering heat treatments. The thermally grown oxide scale is visible as the darker contrast phase between the brighter contrast alloy and coating in the backscatter electron (BSE) SEM images and is composed of Cr, O and Mn according to EDX. The average oxide scale thickness is reported in Table 3 and was determined by measuring every 2 μm along the cross section of at least five different, representative SEM images of the same magnification as shown in Figure 1. EDX analysis was used to confirm the interface between the thermally grown oxide scale and the coating, defining the oxide scale to be the phase containing less than trace amount (0.5 wt.%) of Co. The mass gain of uncoated Crofer 22 APU after the sintering heat treatment is given in Table 3. The corresponding oxide scale thickness in Table 3 was calculated assuming all of the mass gain corresponds to oxygen uptake to form pure Cr_2O_3.

XRD of the coating surface after the three different sintering heat treatments is shown in Figure 2. All diffraction peaks could be indexed to a cubic spinel phase, and are shifted slightly to the left in comparison with $MnCo_2O_4$ (JCPDS card no. 23-1237) The three sintering heat treatments do not result in significant difference in coating composition according to EDX analysis (< 3 wt.% difference on analysis of cations). The average composition is $Mn_{1.1}Co_{1.6}Fe_{0.3}O_4$, i.e. the Mn/Co fraction in the as-sintered coatings is slightly higher compared to the nominal powder composition ($MnCo_{1.7}Fe_{0.3}O_4$). Trace amounts of Cr (< 0.5 wt.%) are detected in all of the coatings.

The porosity of the as-sintered coatings was estimated based on five representative SEM images of the same magnification as in Figure 1a-c) using ImageJ software [37] and is reported in Table 3. Heat treatment in air at 900 °C is only sufficient to initiate neck formation between the ceramic particles (Fig. 1a). The coating detached from the substrate during mounting in epoxy, indicating poor adhesion to the steel and low strength of the coating itself. Heat treatment in reducing atmosphere at 900 °C before re-oxidation in air leads to visible improvements in both densification and adhesion (Fig. 1b). A thin, dense layer appears to cover most of the thermally grown oxide scale, while the porosity of the bulk part of the coating is still high. The increased temperature from 900 °C to 1100 °C during the reduction step improves densification considerably (Fig. 1c). The few remaining pores in the coating appear all to be isolated. The thermally grown oxide scale thickness is increased by nearly a factor of three due to the increased temperature during the reduction heat treatment step (Table 3).

Bright particles were observed in the oxide scale of both samples heat-treated in reducing atmosphere (R900+O800 and R1100+O800). According to EDX point analysis the particles contained more Fe and less O compared to the surrounding scale, indicating that the bright particles are metallic inclusions.

Table 3. Coating porosity and thermally grown oxide scale thickness measured on SEM images of $MnCo_{1.7}Fe_{0.3}O_4$ spinel coated Crofer 22 APU after sintering. Mass gain of uncoated Crofer 22 APU after heat treatment under the same conditions, and calculated Cr_2O_3 thickness based on mass gain.

Sample	Coating porosity [%]	Thermally grown oxide scale thickness [μm]	Mass gain of Crofer 22 APU [mg cm^{-2}]	Calculated Cr_2O_3 thickness [μm]
O900	53±5	0.3±0.2	0.06	0.36
R900+O800	35±5	0.6±0.2	0.10	0.61
R1100+O800	17±3	1.8±0.3	0.56	3.4

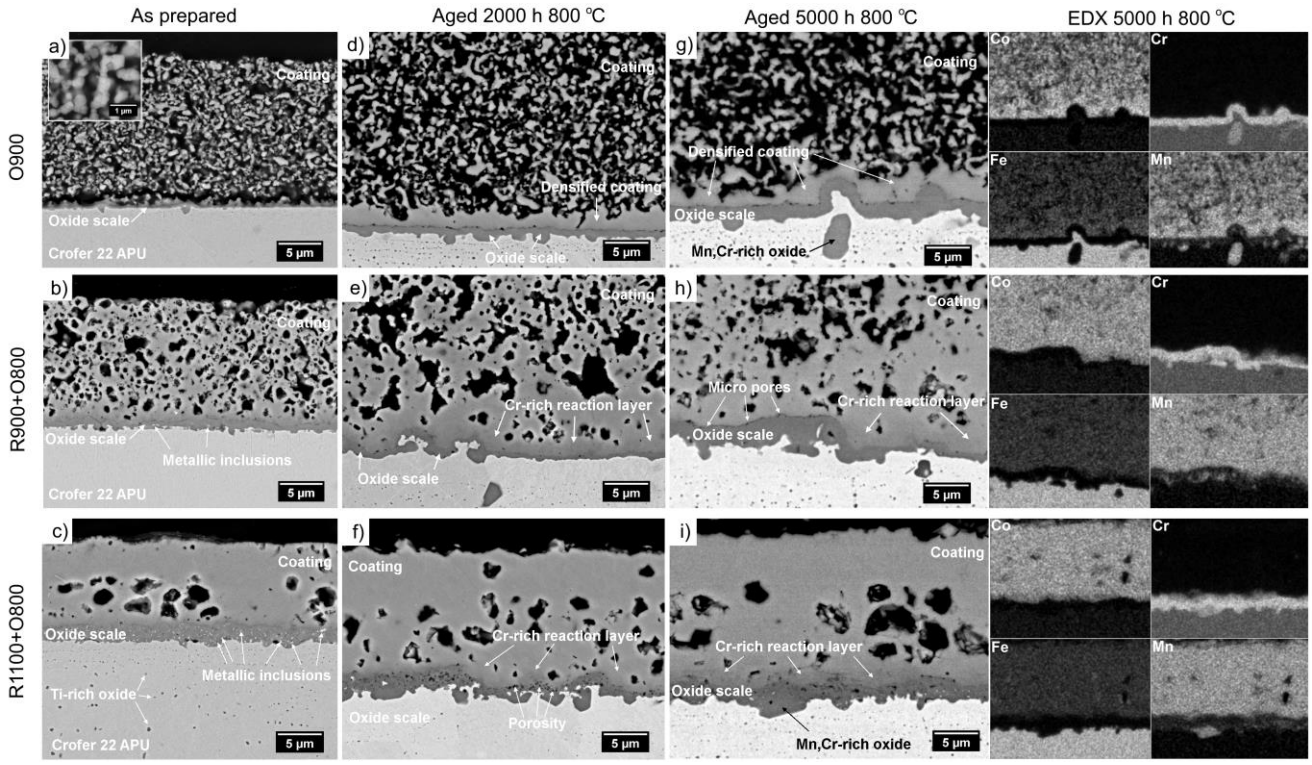

Figure 1. SEM backscatter electron images of $MnCo_{1.7}Fe_{0.3}O_4$ coated Crofer 22 APU, a)-c) After sintering heat treatment, d)-f) After 2000 h oxidation in air at 800 °C, g)-i) After 5000 h oxidation in air at 800 °C and corresponding EDX maps.

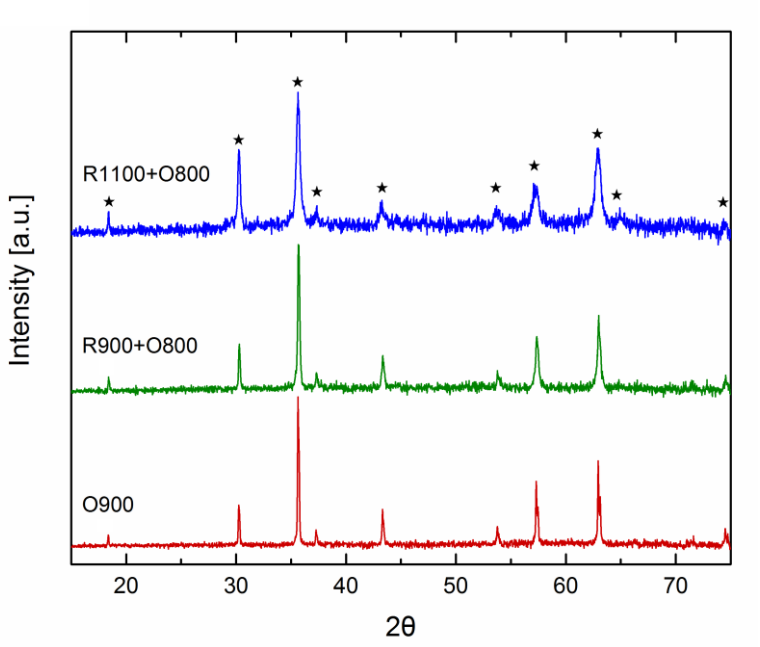

Figure 2. XRD of the coating surface after different sintering heat treatments. Star indicates peaks belonging to a cubic spinel phase.

3.2 Oxidation in air

The mass change of uncoated and $MnCo_{1.7}Fe_{0.3}O_4$ coated Crofer 22 APU measured during oxidation in air at 800 °C is shown in Figure 3a. For all of the coated samples, mass change over time follows to close approximation parabolic oxidation kinetics, described by (2):

$$(\Delta m/A)^2 = k_P t + C \tag{2}$$

where Δm is the measured mass change [g], A is the sample area [cm^2], k_P is the parabolic rate constant [$g^2\ cm^{-4}s^{-1}$], t is the time [s] and C is an integration constant. The mass change of uncoated Crofer 22 APU is parabolic only the first 1000 h of oxidation, after this the mass gain increases. Parabolic oxidation rate constants were obtained from a linear fit of the $(\text{mass gain})^2$ vs time data, shown in Figure 3b, and are summarized in Table 4. The mass gain during the first 250 h was ignored to avoid

potential contributions from continued re-oxidation of the coating or initial non-parabolic oxidation behavior [38]. For uncoated Crofer 22 APU, the mass change between 250 h and 1000 h (parabolic region) was used to determine the rate constant. During the first 250 h of oxidation, the mass gain of the two samples heat-treated under reducing conditions (R900+O800 and R1100+O800) is larger than the mass gain of the sample heat treated in air only (O900). This indicates that the coatings were not completely re-oxidized after the reduction heat treatment, even though XRD of the surface only shows peaks belonging to a cubic spinel. The sample with the densest coating (R1100+O800) displays the lowest oxidation rate, but also the most porous coating (O900) reduces the oxidation rate of Crofer 22 APU.

Table 4. Parabolic oxidation rate constant of uncoated and $MnCo_{1.7}Fe_{0.3}O_4$ coated Crofer 22 APU in air at 800 °C calculated from mass gain measured over 5000 h (coated samples) or 1000 h (uncoated Crofer 22 APU) of oxidation.

Sample	k_p [10^{-14} g^2 $cm^{-4}s^{-1}$]
O900	1.4
R900+O800	1.3
R1100+O800	0.34
Uncoated Crofer 22 APU	4.2

3.3 Cr evaporation

The total amount of chromium species evaporated and the rate of Cr evaporation during continuous exposure to air-3% H_2O is shown in Figure 4a and b, respectively. Note that in both graphs, the first measurement point for the O900 samples corresponds to exposure to 900 °C for 2 h (*in-situ* sintering). During this period the Cr evaporation rate of O900 is the same as the Cr evaporation rate of uncoated Crofer 22 APU measured at 800 °C. After the temperature is lowered to 800 °C, the Cr evaporation

rate of O900 decreases with time and stabilizes at a value ten times lower than measured for uncoated Crofer 22 APU. The evaporation rate from samples with denser coatings (R1100+O800) is nearly constant over time and on average three times lower than measured for the more porous coating (O900).

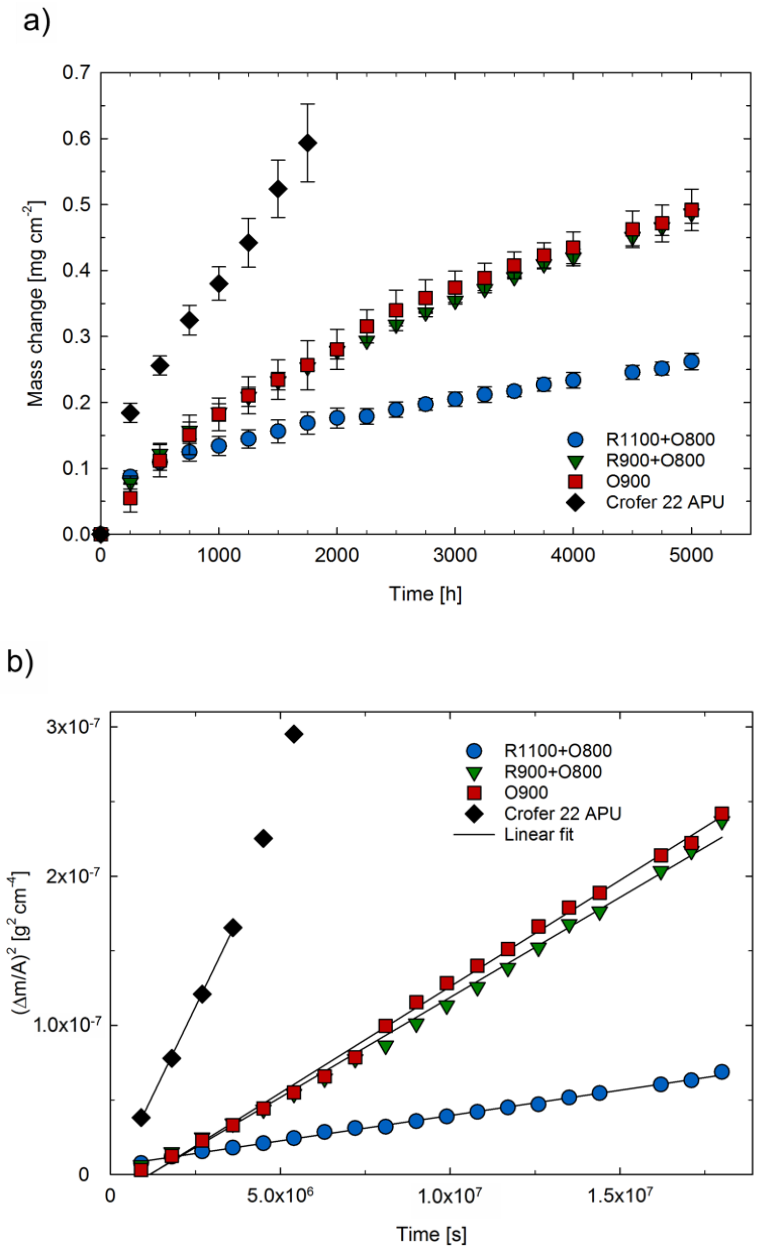

Figure 3. (a) Mass change of uncoated and $MnCo_{1.7}Fe_{0.3}O_4$ coated Crofer 22 APU during cyclic oxidation in air at 800 °C. Each point is the average of 2-5 samples and the error bars are equal to one standard deviation. (b) Parabolic rate plot with lines showing the best linear fit.

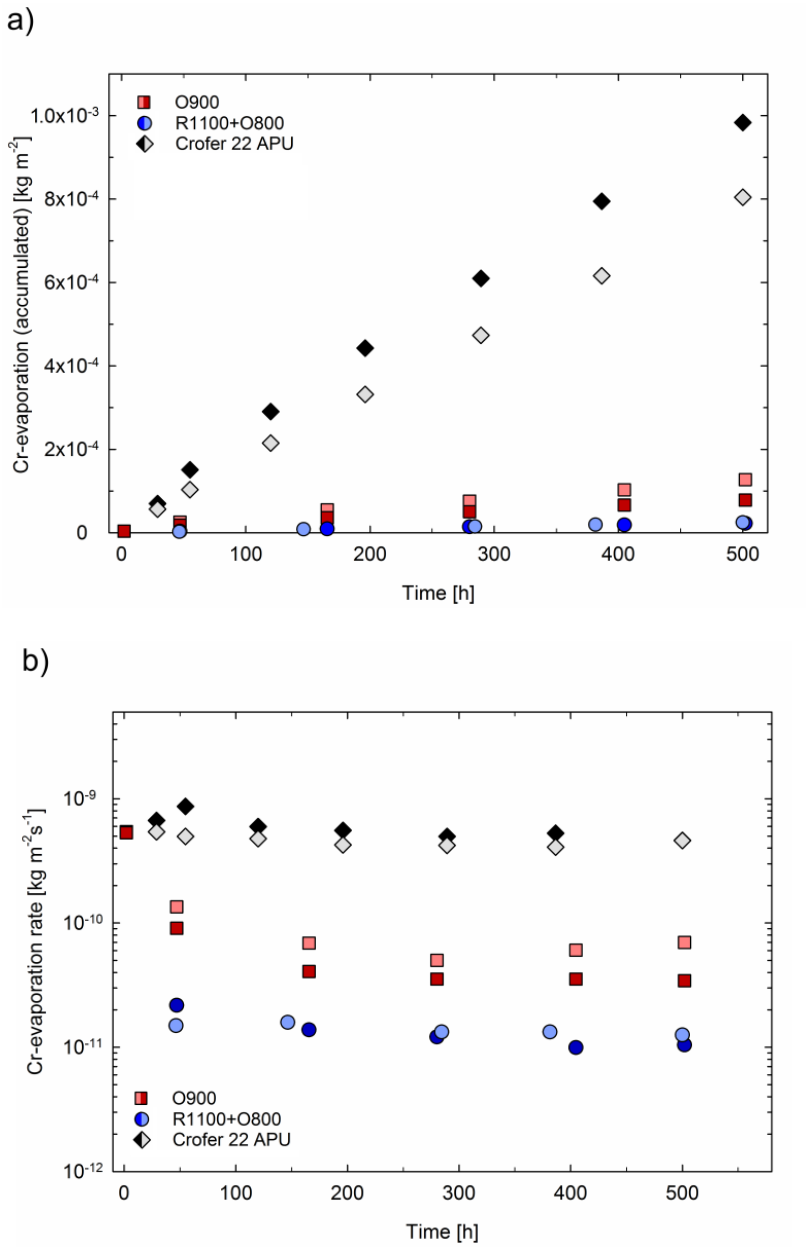

Figure 4. Cr evaporation from uncoated and $MnCo_{1.7}Fe_{0.3}O_4$ coated Crofer 22 APU measured in air-3% H_2O at 800 °C. Results from two measurements in two different furnaces under identical conditions are shown. The first value for the O900 sample (at 2 h exposure time) was measured at 900 °C. () Total amount of Cr-species evaporated (b) Rate of Cr evaporation over time.

3.4 Microstructure after oxidation

The microstructural and compositional development of $MnCo_{1.7}Fe_{0.3}O_4$ coated Crofer 22 APU during oxidation at 800 °C in air is shown in the SEM images and EDX maps in Figure 1d)-i). Along the interface of the intially highly porous coating (O900) and the thermally grown oxide scale, a 2-4 μm dense layer formed after 2000 h of oxidation (Fig. 1d). According to quantitative EDX point analysis the amount of Cr in the densified layer is 3-5 wt.%, while the average amount in the porous portion of the coating is ≤ 1wt.%. There was no measurable differences in the concentration of Co, Mn and Fe in the dense and porous portions of the coating and no difference in composition within the porous part of the coating. The Co/Mn fraction in the whole coating (dense and porous part) decreases with increasing oxidation time from 1.7 in the as-prepared coating, to 1.4 after 2000 h at 800 °C, and finally to1.2 after 5000 h at 800 °C (fractions based on wt.%). The amount of Fe in the coating remaines constant (8±1 wt.%). The O900 samples exposed to air-3% H_2O for 500 h during Cr evaporation measurement had a similar microstructure (not shown). The thickness of the densified region was slightly thinner for these samples, while it does not increase significantly from 2000 to 5000 h of oxidation in air. The adhesion between the O900 coating and the alloy substrate appears to have improved during oxidation as the coating did not detach during mounting in epoxy.

EDX maps of coatings heat treated under reducing atmosphere (R900+O800 and R1100+O800) show a reaction layer consisting of Mn, Cr, Co, Fe and O between the thermally grown oxide scale and spinel coatings (Fig. 1h and i). The thickness of this reaction layer is 3-5 μm, with large variation along the interface, after both 2000 h and 5000 h of oxidation. The variation in reaction layer thickness is generally opposite the variation in oxide scale thickness, i.e. a thinner reaction layer is observed where the oxide scale is thicker and vice versa. In areas where there is no distinct reaction layer visible, micro-pores can be observed along the oxide scale/coating interface. These features are observed for both R900+O800 and R1100+O800 coatings and are most clearly seen in Figure 1h. In areas where the reaction layer was thick, EDX linescans indicated a compositional plateau of 30 wt.%

O, 25 wt.% Cr, 26 wt.% Co, 12 wt.% Mn, and 7 wt.% Fe. Thus, the reaction layer of coatings heat treated under reducing atmosphere (R900+O800 and R1100+O800) contains significantly larger amounts of Cr (up to 25 wt.%) than the densified layer of the O900 coating (up to 5 wt.% Cr). The average Cr content in the coating above the reaction layer, analyzed 7 μm away from the oxide scale/coating interface, is below 1 wt.%.

The thermally grown oxide scale thickness varies along the interface for all samples, but is most uniform for the R900 samples. The average thickness is summarized in Table 5 and was determined by measuring every 2 μm along the cross section of at least five different, representative SEM images at the same magnification as shown in Figure 1. The thickness of the scale under the O900 coating increases at a higher rate than the scale under the R900+O800 coating. The scale thickness under the R1100+O800 coating does not change significantly during oxidation. Figures 1f) and i) show that the scale is more porous after oxidation than it is directly after sintering (Fig. 1c). Metallic inclusions in the scale are still visible, but in lower quantities.

In all of the samples, oxides rich in Mn and Cr were detected at the scale/alloy interface (see EDX maps in Figure 1). Internal oxides rich in Ti were detected further below the alloy surface, and are visible on the SEM backscatter electron images as darker particles in the brighter alloy matrix. No cracking or spallation of the coating or thermally grown oxide scale was observed for any of the samples after oxidation.

Table 5. Average thermally grown oxide scale thickness measured on SEM micrographs of $MnCo_{1.7}Fe_{0.3}O_4$ coated Crofer 22 APU after 2000 h and 5000 h oxidation at 800 °C in air.

	Oxide scale thickness [μm]	
Sample	2000 h	5000 h
O900	0.8±0.3	1.3±0.4
R900+O800	0.8±0.4	1.1±0.6
R1100+O800	1.7±0.7	1.5±0.5

4. Discussion

4.1 Oxidation kinetics

Mass gain during oxidation is a measure of oxygen pick up from the atmosphere, leading to growth of oxide scales and/or internal oxidation. Parabolic mass gain with time, as exhibited by all of the tested samples (Fig. 3), is typically interpreted as oxide scale growth controlled by solid state diffusion through the scale [39]. As the oxide scale grows thicker with time, the diffusion path for the migrating species becomes longer and the mass gain slows down. Figure 3 shows that the R1100+O800 sample has the lowest mass gain during oxidation in air at 800 °C. However, this figure does not take into account the difference in oxide scale thickness among the coated samples after sintering. Because of the higher temperature and longer duration of the sintering heat treatment, the oxide scale on the R1100+O800 sample is three times thicker than the oxide scale on the R900+O800 sample (compare Fig. 1b and c).

To account for differences in starting oxide scale thickness, the mass change results are recalculated by adding the mass gain during sintering to the mass gain measured at 800 °C. The mass gain of

uncoated Crofer 22 APU (Table 2) was used as an estimate for the mass gain during sintering heat treatment, as it was difficult to determine this accurately for the coated samples. Thus, it is assumed that the coating does not provide any significant protection during sintering. This was found to be a fair assumption when comparing the oxide scale thickness of uncoated and coated Crofer 22 APU after the same heat treatment. In addition to calculating the total mass gain, we adjust for the "equivalent age" of the samples after the sintering heat treatment. The equivalent age is here defined as the time uncoated Crofer 22 APU is oxidized at 800 °C before the mass gain of the sintering heat treatment is reached. For example, to achieve the same mass gain as during the R1100+O800 heat treatment (0.56 mg cm^{-2}), uncoated Crofer 22 APU was oxidized for approximately 1650 h at 800 °C in air (see Fig. 3a). Thus, the equivalent age of the R1100+O800 sample after sintering is 1650 h.

The results of the recalculation are shown in Figure 5. The *total* mass gain of the R1100+O800 sample is 10 % higher than the *total* mass gain of the O900 sample after 5000 h at 800 °C. This corresponds well with the difference in oxide scale thickness measured on SEM cross sections (Table 5). Nevertheless, the R1100+O800 sample a lower *rate* of oxidation than the O900 sample. Consequentially, the total mass gain of R1100+O800 should become lower than the total mass gain of O900 after a certain period of time. To estimate when this will occur, the mass gain beyond 5000 h was calculated using the parabolic rate constants in Table 4. The results are plotted as lines in Figure 5 and indicate that the same total mass gain should be reached after approximately 15 000 h at 800 °C in air. Hence, the first 15 000 h the interconnect alloy will be less degraded (as expressed by total mass gain) with the O900 coating, whereas after this point, the alloy with the R1100+O800 coating will be less degraded. Considering the target lifetime of SOFCs usually is > 40 000 h, this extrapolation analysis points to that the denser coating will provide a small benefit on the long term oxidation resistance. The oxidation rate is reduced enough to make up for the more severe initial oxidation of the alloy that occurs at the high temperature needed to sinter the coating. However, in the long run, the difference in mass gain due to different coating densities is minor compared to the large reduction in mass gain of Crofer 22 APU provided by the $MnCo_{1.7}Fe_{0.3}O_4$ spinel coating in any form.

The initial porosity of the O900 and R900+O800 coatings is above the 30 % proposed as minimum for physical gas permeability in similar systems [40,41]. Consequently, none of them initially provide a proper physical barrier against the oxidizing gas. However, with time the coatings densified in a 2-4 µm thick region above the thermally grown oxide scale. This densified layer is believed to be responsible for the improved oxidation resistance by reducing the oxygen partial pressure at the oxide scale/coating interface, thereby decreasing the driving force for oxidation [42]. The lower oxidation rate with the denser R1100+O900 coating can be attributed to the presence of a dense $MnCo_{1.7}Fe_{0.3}O_4$ layer above the densified reaction layer. A contributing factor to the lower oxidation rate could be that the high temperature heat treatment used to sinter the coating has modified the properties of the thermally grown oxide scale and thereby affected the oxidation kinetics. It is know that diffusion in Cr_2O_3 can vary with grain size and presence of minor impurities [43,44]. There is however limited information available on how pre-oxidation of Crofer 22 APU at different temperatures and in different atmospheres affects subsequent oxidation behavior in air [45,46]. This will be further investigated in a future study.

It is important to note that the above analysis is based on oxidation in air at 800 °C. It is known that the oxidation rate of ferritic stainless steels decreases 10-30 times by a 100 °C reduction in the oxidation temperature [12,47,48]. Thus, if the SOFC operating temperature is decreased below 800 °C, the R1100+O800 sintering heat treatment will lead to an overall larger degradation of the ferritic stainless steel interconnect also in the long run. On the other hand, decreasing the temperature could result in less densification of the initially highly porous coatings. Without this densified layer, the coating is not expected to improve the oxidation resistance.

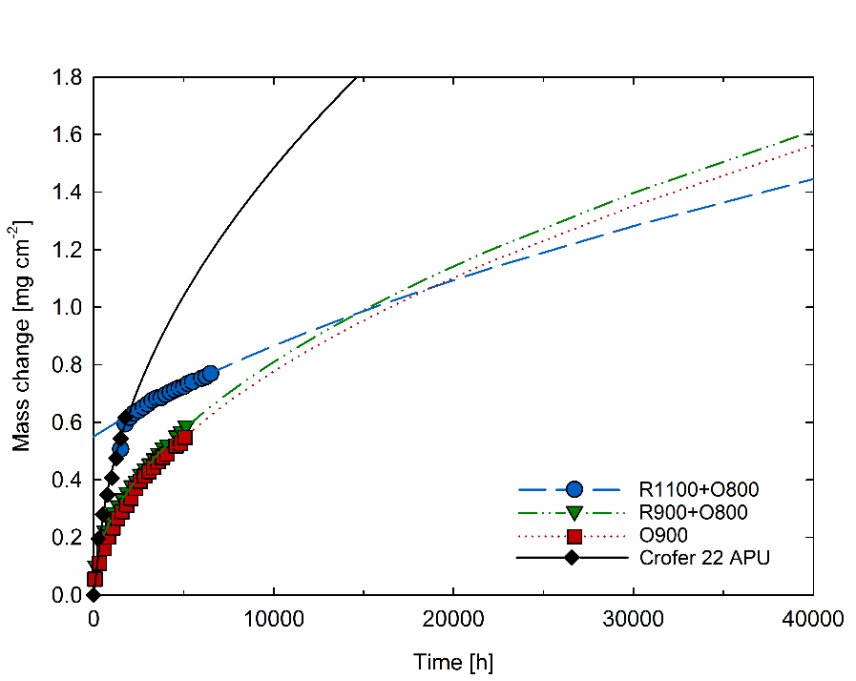

Figure 5. Mass change of uncoated and $MnCo_{1.7}Fe_{0.3}O_4$ coated Crofer 22 APU at 800 °C in air recalculated to include mass change and "equivalent age" of samples after sintering heat treatment. Lines show an extrapolation of the mass change based on the parabolic rate constants.

4.2 Cr evaporation

The denser $MnCo_{1.7}Fe_{0.3}O_4$ coating (R1100+O800) reduced the Cr evaporation rate of Crofer 22 APU by a factor of 37 (Fig. 3b), which is in line with what has previously been reported for $(Mn,Co)_3O_4$ coatings [13,21,49]. The Cr evaporation rate with the R1100+O800 coating is nearly a factor of 10 larger than reported for Co coated Crofer 22 APU in air with 1.88 % H_2O at 800 °C [50]. Some of this difference is likely due to the differences in measurement technique, flow rate and humidity content, making it difficult to conclude on which coating is more effective. It should also be mentioned that approximately 1 % of the surface area of the tested samples was without coating due to coverage by the electrode clip during EPD. Assuming this area has the same Cr evaporation rate as uncoated Crofer

22 APU, it could make up to 45 % of the measured Cr evaporation for the R1100+O800 samples. Differences in the exact size of this area vary slightly from sample to sample, which can account for the measurement scatter.

Nevertheless, since EDX analysis after oxidation showed up to 1 wt.% Cr in the bulk of the coating, some of the collected Cr must have diffused through the coating. Other longer term studies at 800 °C have also reported up to 1 wt.% incorporation of Cr in the $(Mn,Co)_3O_4$ spinel coating close to the air interface [15,51]. Thus, although the $MnCo_{1.7}Fe_{0.3}O_4$ coating obviously is highly effective in reducing Cr volatilization, it does not completely block Cr outward diffusion.

While the denser coating (R1100+O800) provided a better protection against Cr volatilization, even the highly porous coating (O900) reduced the Cr evaporation rate of Crofer 22 APU by a factor of 10. The decreasing Cr evaporation rate over time, and the observation that a dense layer gradually forms between the chromia scale and otherwise porous coating over 500 h of exposure, indicates that the protective action is due to this thin densified layer. Outward diffusing Cr from the alloy reacts with the $MnCo_{1.7}Fe_{0.3}O_4$ spinel coating, thus reducing the amount of Cr released to the atmosphere. It has been shown that Cr diffusion through a $(Mn,Co,Fe,Cr)_3O_4$ reaction layer is slower than diffusion through the $(Mn,Cr)_3O_4$ spinel that typically forms on the outer surface of Crofer 22 APU [52]. The even lower Cr evaporation rate with a dense coating can be attributed to the presence of the denser $MnCo_{1.7}Fe_{0.3}O_4$ layer above a Cr containing reaction layer, acting as further barrier against Cr outward diffusion.

Kurokawa et al. [13] has previously reported that a highly porous $MnCo_2O_4$ coating can reduce Cr vaporization. In their study a highly dense coating was ten times more effective while we found the difference to be only a factor of three. It should be mentioned that the measurements of Kurokawa were performed with a higher content of H_2O in the gas (10 %), which is known to increase the rate of Cr vaporization [53,54]. Nevertheless, since the Cr evaporation rates reported for the bare alloy (9.8×10^{-10} kg $m^{-2}s^{-1}$) and with a highly dense spinel coating (2.3×10^{-11} kg $m^{-2}s^{-1}$) are comparable to

those measured in the current work, it is interesting to compare the results for the more porous coatings as well. The Cr evaporation rate we measured for the porous coated sample (O900) after 47 h of exposure is three times lower than that reported by Kurokawa et al. after 72 h at the same temperature. Kurokawa et al. used the same sintering heat treatment for all samples, the difference in coating density was attributed to different particle size distributions in the spinel powders used to fabricate the coatings. Powder prepared by co-precipitation and calcined at 800 °C had a finer particle size (ca. 0.3 µm) and thus better sinterability than powder prepared by GNP and calcined at 1100 °C (particle size 0.3-3 µm). No dense layer between the coating and chromia scale is visible in their SEM micrographs of the porous coating after exposure, which strengthens the hypothesis that the formation of a dense layer between the thermally grown oxide scale and otherwise porous coating is critical for the coatings protective abilities.

4.3 Microstructural development

The $MnCo_{1.7}Fe_{0.3}O_4$ coating density increased by more than 25 % after heat-treating in N_2-H_2 at 900 °C compared to when heat-treating in air at the same temperature. This is in accordance with previous studies, where improved densification in reducing atmosphere was attributed to a reaction-sintering type mechanism [22,29]. The bright particles observed in the thermally grown oxide scale are metallic inclusions, caused by stress build-up due to internal oxidation [55]. For Crofer 22 APU, internal oxidation of Ti and $(Mn,Cr)_3O_4$ formation at the scale/alloy interface are likely origins of the stress build-up [30,56]. Although manganese chromium oxide usually is reported to form above the chromia scale during oxidation of Crofer 22 APU and similar alloys, the $MnCr_2O_4$ composition has previously been observed at the alloy/scale interface [51,56]. Thermodynamically, $MnCr_2O_4$ is stable down to lower oxygen partial pressures than Cr_2O_3, i.e. $MnCr_2O_4$ is the more stable oxide at the alloy/scale interface [57,58]. The reason why $(Mn,Cr)_3O_4$ also forms at the scale/atmosphere interface has been attributed to the high oxygen affinity of Mn^{2+} and the greater diffusivity of Mn^{2+} compared to Cr^{3+} in thermally grown chromia [59,60].

The initially highly porous O900 and R900+O800 coatings densified with time in vicinity of the thermally grown oxide scale. It is improbable that continued normal sintering is responsible for this densification, as the temperature during aging is low (800 °C) and densification is restricted to a narrow region above the scale. Molin et al. [18] observed similarly that an initially highly porous $MnCo_2O_4$ coating densified near the thermally grown oxide interface after 5000 h aging at 750 °C. The porous coatings were in Molin's case [18] impregnated with Mn and Co nitrates and the nano-particles formed on heating likely facilitated the densification. Here, where oxidation is carried out at a slightly higher temperature of 800 °C, a similar densification at the interface between the thermally grown oxide scale and the coating is observed without an impregnation pre-treatment.

Given that the densified layer of the R900+O800 coating contained up to 25 wt.% of Cr, densification can be attributed to the volume expansion associated with incorporation of Cr from the alloy/oxide scale into the coating. The same explanation cannot not apply for densification of the O900 coating, since in this case the densified region contained less than 5 wt.% Cr. The Mn content in the O900 coating had increased after oxidation compared to in the as-prepared state, which can only be due to diffusion of Mn from the alloy. Although there were no detectable differences in the Co/Mn ratio between the dense and porous parts of the coating, it is possible that the local densification of the O900 coating in part is due to reaction with outward diffusing Mn. Higher resolution microscopy will be necessary to investigate this mechanism further.

The large difference in Cr concentration in the densified regions of the R900+O800 and O900 coatings may be explained on basis of the compositional changes taking place during the two sintering heat treatments. The microstructural development of the coatings from deposition to long term aging at 800 °C in air is summarized schematically in Figure 6. Gambino et al. [30] showed that during heat treatment of $Mn_{1.5}Co_{1.5}O_4$ coated Crofer 22 APU in N_2-H_2 at 900 °C, the $Mn_{1.5}Co_{1.5}O_4$ coating is reduced to MnO and Co, as expected from the phase diagram for this system [61]. Simultaneously, a

ca. 3 µm thick Cr_2O_3 + $(Mn,Cr)_3O_4$ scale forms at the coating/alloy interface [30]. After a re-oxidation heat treatment, a reaction layer comprising Mn, Cr, Co and Fe is detected between the oxide scale and the re-oxidized coating [51]. The oxide scale now consists of primarily Cr_2O_3. Thus, during re-oxidation, Mn in $(Mn,Cr)_3O_4$ is partially replaced by Co and Fe to form a Cr-rich reaction layer.

Based on results in the current study, it is argued that the formation of $(Mn,Cr)_3O_4$ is a prerequisite for the formation of the Cr-rich reaction layer. Gambino et al. [30] proposed that Cr_2O_3 is formed first on Crofer 22 APU and that the $(Mn,Cr)_3O_4$ spinel grows with time due to outward diffusion of Mn from the alloy. We suggest that a contributing factor to the growth of $(Mn,Cr)_3O_4$ during the reduction heat treatment step is reaction between thermally grown Cr_2O_3 on the alloy and MnO from the reduced coating. This reaction would allow for the formation of a thicker spinel layer due to the more accessible source of Mn. The low amount of Cr in the densified layer of the O900 coating is thus due to limited growth of $(Mn,Cr)_3O_4$. Since this coating is not reduced to MnO and Co, $(Mn,Cr)_3O_4$ can only form by diffusion of Mn from the alloy. In contrast, the reaction layer of the R900+O800 coated sample contains more Cr due to the initial formation of a thicker $(Mn,Cr)_3O_4$ layer, which reacts with Co and Fe from the coating during re-oxidation.

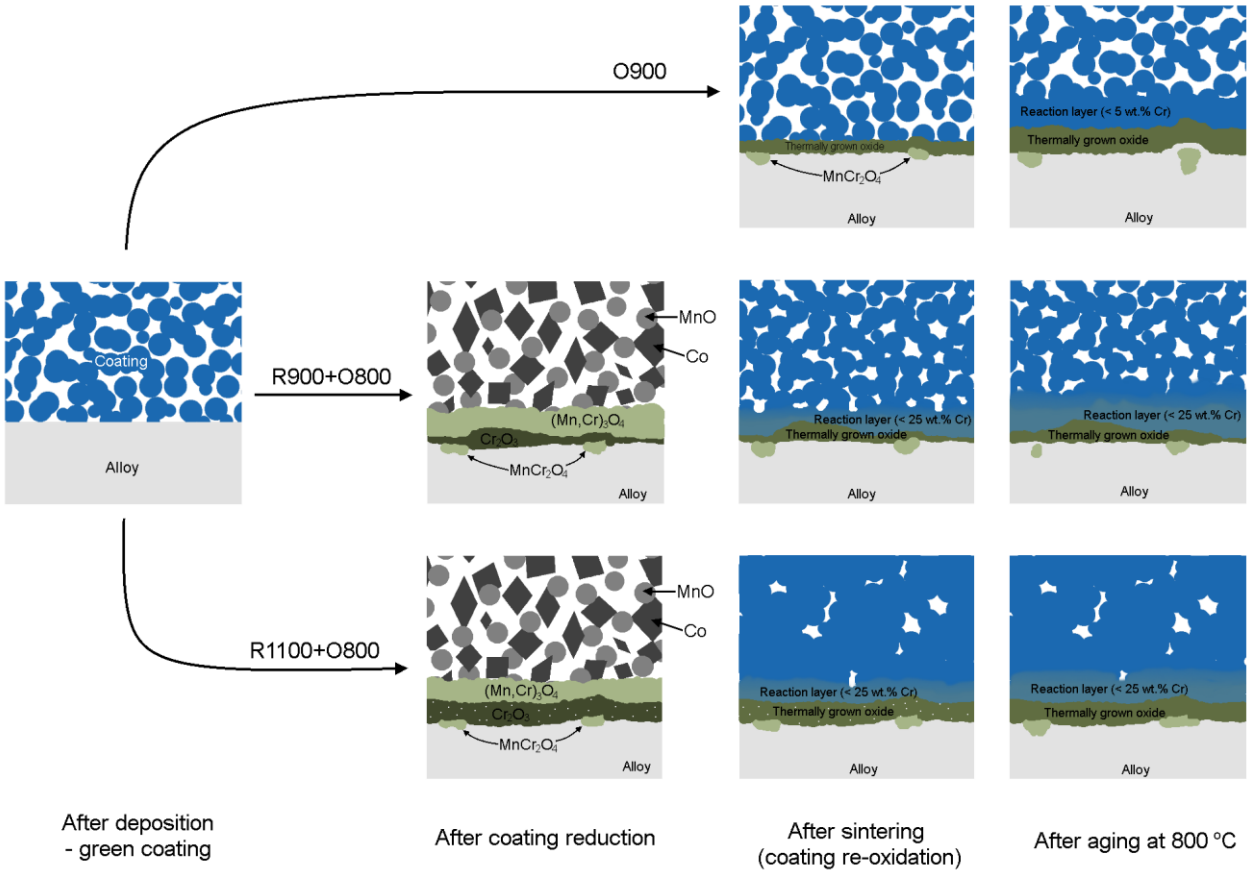

Figure 6. Schematic illustration of the microstructural development during sintering heat treatment and oxidation aging of spinel coated Crofer 22 APU. Iron in the coating has been omitted for simplicity. The thermally grown oxide scale consists of Cr, O and Mn.

4.4 Implications for long-term performance as protective coatings

One way of evaluating the lifetime of interconnect alloys is based on the time it takes to decrease the concentration of Cr in the alloy beneath a critical level where break-away oxidation may occur. This can be used as a criterion for determining whether the spinel coating is protective enough. For ferritic stainless steels such as Crofer 22 APU, the critical Cr concentration before break-away has been determined to be approximately 16 wt.% [10]. Quadakkers et al. [62] derived an expression for the time to break-away for alumina forming steel, which Huczkowski et al. [10] later showed was

applicable for chromia forming alloys. For a rectangular sheet of infinite width and breadth, it can be shown that the time to break-away is given by:

$$t_B = \left\{\left[(C_0 - C_B) \cdot \rho_{alloy} \cdot d \cdot 2.3 \cdot 10^{-3}\right] - w_{pre}\right\}^2 \cdot 1/k_P \quad (3)$$

where C_0 and C_B are the initial and final Cr-concentrations in the alloy, ρ_{alloy} is the density of the alloy, d is the alloy thickness, w_{pre} is the initial mass gain during sintering of the coating and k_P is the parabolic rate constant. In the following, it is assumed that all of the measured mass gain is due to oxidation of Cr to Cr_2O_3, that oxide spallation does not occur and that k_P is independent of the component thickness. For oxidation of uncoated Crofer 22 APU at 800 °C the last assumption has been found to be valid as long as the thickness is between 0.3 and 2 mm; below this the parabolic rate constant increases with decreasing alloy thickness [10].

Figure 7 shows the time to break-away with the different coatings as a function of alloy thickness. The calculations indicate that based on a Cr depletion criterion, a plate of Crofer 22 APU with the most porous spinel coating (O900) only needs to be > 0.15 mm thick to withstand 40 000 h at 800 °C. Without any coating, the required thickness nearly doubles. This is without taking evaporation of the scale into account. Sachitanand et al. [11] has shown that the time for break-away of 0.2 mm thick Sandvik HT at 850 °C decreases by a factor of two when exposed to high flow rate conditions, compared to when Cr evaporation is suppressed. Although Cr evaporation will decrease the lifetime of the porous coated samples as well, the influence will be considerably smaller due to the 10 times lower Cr evaporation rate compared to uncoated Crofer 22 APU.

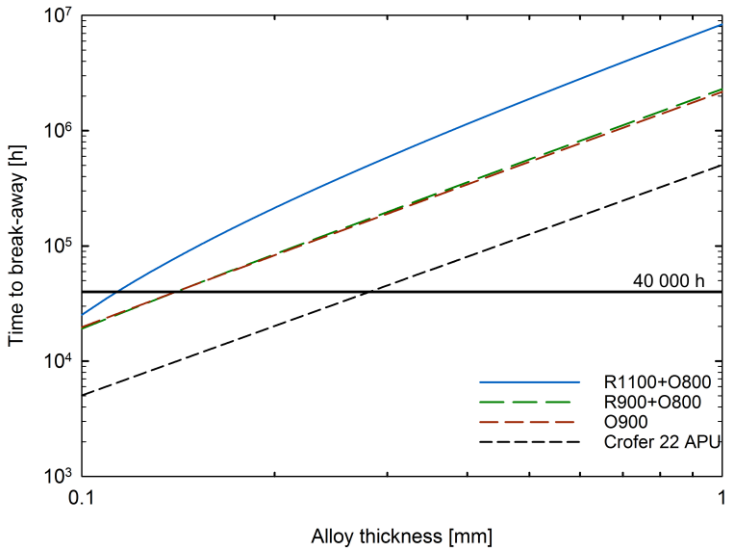

Figure 7. Time to break-away oxidation as a function of component thickness for uncoated and spinel coated Crofer 22 APU calculated based on measured oxidation rate at 800 °C in air. The black horizontal line marks 40 000 h.

Based on the oxidation behavior and from a Cr-depletion perspective alone it can be concluded that even an initially highly porous $MnCo_{1.7}Fe_{0.3}O_4$ coating, which results from heat treatment in air at 900 °C, will provide sufficient protection of an interconnect alloy like Crofer 22 APU to meet SOFC lifetime requirements. The predicted mass gain difference between the dense and porous coating is less than 10 % after 40 000 h (Fig. 5), which is not expected to result in a significant difference in ASR as this is mainly a function of the oxide scale thickness and conductivity [4]. In terms of thermo-mechanical properties, porous coatings could prove to be superior to dense by providing some strain tolerance, if sufficient adherence between coating and steel is ensured over the first few hundred hours of stack use [29,63]. Also, the ease with which a good electrical contact between the electrode and the coated interconnect can be established will differ between the porous and dense coating.

The main uncertainty with the use of porous coatings is whether the higher rate of Cr evaporation will lead to unacceptably high degradation of the SOFC cathode. Stanislowski et al. [50] estimated that for

every 3.96 µg cm^{-2} of Cr released from the interconnect, the cell voltage of a typical SOFC stack with a $La_xSr_yMnO_3$ (LSM) cathode operated at Research Center Juelich would degrade by 1 %. From the measured Cr-vaporization rates in the current study, this corresponds to a cell voltage degradation rate of 43 %/1000 h for uncoated Crofer 22 APU, 4.7 %/1000 h with the coating sintered in air (O900) and 1.7 %/1000 h with the coating sintered by the two-step procedure (R1100+O800). The estimated degradation rates indicate that not even the highly dense coating is protective enough. More recent SOFC stack tests at Juelich show a cell voltage degradation rate of only 0.5 %/1000 h with Crofer 22 APU coated with $MnCo_{1.9}Fe_{0.1}O_4$ by atmospheric plasma spraying (stack operated with $La_{0.65}Sr_{0.3}MnO_3$ cathode and $La(Mn,Cu,Co)O_3$ contact at 800 °C, 0.5 A cm^{-2}, 39.8 % fuel utilization) [14,64]. Degradation by Cr poisoning is a complex issue, which depends among other factors on the cathode material, operating temperature, and current density [65]. It has been questioned whether a direct correlation exist between the cell degradation rate and the amount of Cr deposited [66]. Thus, the question about whether the here applied highly porous coating provides sufficient reduction of Cr evaporation for operation in current state-of-the-art stacks remains to be resolved.

5. Conclusion

The effect of $MnCo_{1.7}Fe_{0.3}O_4$ coating density on the oxidation kinetics and Cr evaporation rate of Crofer 22 APU was assessed. Denser coatings were achieved with a two-step reduction and re-oxidation heat treatment, compared to heat treating in air only. However, the initially highly porous air sintered coatings densified with time during aging at 800 °C in air.

The initial coating density did not have major influence on the long-term oxidation behavior in air at 800 °C. If the lifetime is assessed on a Cr-depletion criterion alone, it was shown that even an air

sintered $MnCo_{1.7}Fe_{0.3}O_4$ spinel coating provides sufficient protection of Crofer 22 APU to survive 40 000 h service at 800 °C when the interconnect thickness is above 0.15 mm. The potentially largest drawback with a porous, air-treated coating is the higher Cr evaporation rate. Although the Cr evaporation rate was reduced 10 times relative to uncoated Crofer 22 APU, it was still 3-4 times higher than what was measured for the dense coating. The protective action of this initially highly porous coating was attributed to partial densification of the coating in vicinity of the thermally grown oxide scale.

Funding: This research did not receive any specific grant from funding agencies in the public, commercial, or not-for-profit sectors.

References

[1] W.Z. Zhu, S.C. Deevi, Development of interconnect materials for solid oxide fuel cells, Materials Science and Engineering: A. 348 (2003) 227–243. doi:10.1016/S0921-5093(02)00736-0.

[2] S. Linderoth, P.V. Hendriksen, M. Mogensen, N. Langvad, Investigations of metallic alloys for use as interconnects in solid oxide fuel cell stacks, Journal of Materials Science. 31 (1996) 5077–5082. doi:10.1007/BF00355908.

[3] J.W. Fergus, Metallic interconnects for solid oxide fuel cells, Materials Science and Engineering: A. 397 (2005) 271–283. doi:10.1016/j.msea.2005.02.047.

[4] W.Z. Zhu, S.C. Deevi, Opportunity of metallic interconnects for solid oxide fuel cells: a status on contact resistance, Materials Research Bulletin. 38 (2003) 957–972. doi:10.1016/S0025-5408(03)00076-X.

[5] K. Hilpert, D. Das, M. Miller, D.H. Peck, R. Weiß, Chromium Vapor Species over Solid Oxide Fuel Cell Interconnect Materials and Their Potential for Degradation Processes, J. Electrochem. Soc. 143 (1996) 3642–3647. doi:10.1149/1.1837264.

[6] J.W. Fergus, Effect of cathode and electrolyte transport properties on chromium poisoning in solid oxide fuel cells, International Journal of Hydrogen Energy. 32 (2007) 3664–3671. doi:10.1016/j.ijhydene.2006.08.005.

[7] L. Zhao, S. Amarasinghe, S.P. Jiang, Enhanced chromium tolerance of $La_{0.6}Sr_{0.4}Co_{0.2}Fe_{0.8}O_{3-\delta}$ electrode of solid oxide fuel cells by $Gd_{0.1}Ce_{0.9}O_{1.95}$ impregnation, Electrochemistry Communications. 37 (2013) 84–87. doi:10.1016/j.elecom.2013.10.019.

[8] E. Park, S. Taniguchi, T. Daio, J.-T. Chou, K. Sasaki, Comparison of chromium poisoning among solid oxide fuel cell cathode materials, Solid State Ionics. 262 (2014) 421–427. doi:10.1016/j.ssi.2014.01.047.

[9] M. Yang, E. Bucher, W. Sitte, Effects of chromium poisoning on the long-term oxygen exchange kinetics of the solid oxide fuel cell cathode materials $La_{0.6}Sr_{0.4}CoO_3$ and Nd_2NiO_4, Journal of Power Sources. 196 (2011) 7313–7317. doi:10.1016/j.jpowsour.2010.10.064.

[10] P. Huczkowski, V. Shemet, J. Piron-Abellan, L. Singheiser, W.J. Quadakkers, N. Christiansen, Oxidation limited life times of chromia forming ferritic steels, Materials and Corrosion. 55 (2004) 825–830. doi:10.1002/maco.200303798.

[11] R. Sachitanand, J.-E. Svensson, J. Froitzheim, The Influence of Cr Evaporation on Long Term Cr Depletion Rates in Ferritic Stainless Steels, Oxid Met. 84 (2015) 241–257. doi:10.1007/s11085-015-9552-5.

[12] H. Falk-Windisch, J.E. Svensson, J. Froitzheim, The effect of temperature on chromium vaporization and oxide scale growth on interconnect steels for Solid Oxide Fuel Cells, Journal of Power Sources. 287 (2015) 25–35. doi:10.1016/j.jpowsour.2015.04.040.

[13] H. Kurokawa, C.P. Jacobson, L.C. DeJonghe, S.J. Visco, Chromium vaporization of bare and of coated iron–chromium alloys at 1073 K, Solid State Ionics. 178 (2007) 287–296. doi:10.1016/j.ssi.2006.12.010.

[14] J. Malzbender, P. Batfalsky, R. Vaßen, V. Shemet, F. Tietz, Component interactions after long-term operation of an SOFC stack with LSM cathode, Journal of Power Sources. 201 (2012) 196–203. doi:10.1016/j.jpowsour.2011.10.117.

[15] J.W. Stevenson, Z.G. Yang, G.G. Xia, Z. Nie, J.D. Templeton, Long-term oxidation behavior of spinel-coated ferritic stainless steel for solid oxide fuel cell interconnect applications, Journal of Power Sources. 231 (2013) 256–263. doi:10.1016/j.jpowsour.2013.01.033.

[16] Y. Larring, T. Norby, Spinel and Perovskite Functional Layers Between Plansee Metallic Interconnect (Cr-5 wt % Fe-1 wt % Y_2O_3) and Ceramic $(La_{0.85}Sr_{0.15})_{0.91}MnO_3$ Cathode Materials for Solid Oxide Fuel Cells, J. Electrochem. Soc. 147 (2000) 3251–3256. doi:10.1149/1.1393891.

[17] F. Smeacetto, A. De Miranda, S. Cabanas Polo, S. Molin, D. Boccaccini, M. Salvo, A.R. Boccaccini, Electrophoretic deposition of $Mn_{1.5}Co_{1.5}O_4$ on metallic interconnect and interaction with glass-ceramic sealant for solid oxide fuel cells application, Journal of Power Sources. 280 (2015) 379–386. doi:10.1016/j.jpowsour.2015.01.120.

[18] S. Molin, P. Jasinski, L. Mikkelsen, W. Zhang, M. Chen, P.V. Hendriksen, Low temperature processed MnCo2O4 and MnCo1.8Fe0.2O4 as effective protective coatings for solid oxide fuel cell interconnects at 750 °C, Journal of Power Sources. 336 (2016) 408–418. doi:10.1016/j.jpowsour.2016.11.011.

[19] Å.H. Persson, L. Mikkelsen, P.V. Hendriksen, M.A.J. Somers, Interaction mechanisms between slurry coatings and solid oxide fuel cell interconnect alloys during high temperature oxidation, Journal of Alloys and Compounds. 521 (2012) 16–29. doi:10.1016/j.jallcom.2011.12.095.

[20] L. Chen, E.Y. Sun, J. Yamanis, N. Magdefrau, Oxidation Kinetics of $Mn_{1.5}Co_{1.5}O_4$-Coated Haynes 230 and Crofer 22 APU for Solid Oxide Fuel Cell Interconnects, J. Electrochem. Soc. 157 (2010) B931–B942. doi:10.1149/1.3391820.

[21] R. Trebbels, T. Markus, L. Singheiser, Investigation of Chromium Vaporization From Interconnector Steels With Spinel Coatings, J. Fuel Cell Sci. Technol. 7 (2009) 011013–011013. doi:10.1115/1.3117607.

[22] S.-I. Lee, J. Hong, H. Kim, J.-W. Son, J.-H. Lee, B.-K. Kim, H.-W. Lee, K.J. Yoon, Highly Dense Mn-Co Spinel Coating for Protection of Metallic Interconnect of Solid Oxide Fuel Cells, J. Electrochem. Soc. 161 (2014) F1389–F1394. doi:10.1149/2.0541414jes.

[23] M. Mirzaei, A. Simchi, M.A. Faghihi-Sani, A. Yazdanyar, Electrophoretic deposition and sintering of a nanostructured manganese–cobalt spinel coating for solid oxide fuel cell interconnects, Ceramics International. 42 (2016) 6648–6656. doi:10.1016/j.ceramint.2016.01.012.

[24] Y. Zhang, A. Javed, M. Zhou, S. Liang, P. Xiao, Fabrication of Mn–Co Spinel Coatings on Crofer 22 APU Stainless Steel by Electrophoretic Deposition for Interconnect Applications in Solid Oxide Fuel Cells, Int. J. Appl. Ceram. Technol. 11 (2014) 332–341. doi:10.1111/ijac.12013.

[25] M.R. Bateni, P. Wei, X. Deng, A. Petric, Spinel coatings for UNS 430 stainless steel interconnects, Surface and Coatings Technology. 201 (2007) 4677–4684. doi:10.1016/j.surfcoat.2006.10.011.

[26] E. Saoutieff, G. Bertrand, M. Zahid, L. Gautier, APS Deposition of $MnCo_2O_4$ on Commercial Alloys K41X used as Solid Oxide Fuel Cell Interconnect: The Importance of Post Heat-treatment for Densification of the Protective Layer, ECS Trans. 25 (2009) 1397–1402. doi:10.1149/1.3205670.

[27] J. Puranen, M. Pihlatie, J. Lagerbom, T. Salminen, J. Laakso, L. Hyvärinen, M. Kylmälahti, O. Himanen, J. Kiviaho, P. Vuoristo, Influence of powder composition and manufacturing method on electrical and chromium barrier properties of atmospheric plasma sprayed spinel coatings prepared from $MnCo_2O_4$ and Mn_2CoO_4 + Co powders on Crofer 22 APU interconnectors, International Journal of Hydrogen Energy. 39 (2014) 17246–17257. doi:10.1016/j.ijhydene.2014.08.016.

[28] L. Besra, M. Liu, A review on fundamentals and applications of electrophoretic deposition (EPD), Progress in Materials Science. 52 (2007) 1–61. doi:10.1016/j.pmatsci.2006.07.001.

[29] Z. Yang, G. Xia, S.P. Simner, J.W. Stevenson, Thermal Growth and Performance of Manganese Cobaltite Spinel Protection Layers on Ferritic Stainless Steel SOFC Interconnects, J. Electrochem. Soc. 152 (2005) A1896–A1901. doi:10.1149/1.1990462.

[30] L.V. Gambino, N.J. Magdefrau, M. Aindow, Microstructural effects of the reduction step in reactive consolidation of manganese cobaltite coatings on Crofer 22 APU, Materials at High Temperatures. 32 (2015) 142–147. doi:10.1179/0960340914Z.00000000090.

[31] N.J. Magdefrau, L. Chen, E.Y. Sun, M. Aindow, The effect of $Mn_{1.5}Co_{1.5}O_4$ coatings on the development of near surface microstructure for Haynes 230 oxidized at 800 °C in air, Surface and Coatings Technology. 242 (2014) 109–117. doi:10.1016/j.surfcoat.2014.01.025.

[32] N.J. Kidner, Nextech Coatings, Protective Coatings for Metallic SOFC Components, (2012). http://www.netl.doe.gov/File%20Library/events/2012/13th%20annual%20seca%20workshop/Kidner.pdf.

[33] S.R. Akanda, N.J. Kidner, M.E. Walter, Spinel coatings on metallic interconnects: Effect of reduction heat treatment on performance, Surface and Coatings Technology. 253 (2014) 255–260. doi:10.1016/j.surfcoat.2014.05.049.

[34] B. Talic, PhD Thesis. Metallic Interconnects for Solid Oxide Fuel Cells: High Temperature Corrosion and Protective Spinel Coatings, Norwegian University of Science and Technology, 2016. https://brage.bibsys.no/xmlui/handle/11250/2404554.

[35] Thyssen Krupp, Crofer 22 APU Material Data Sheet No. 4046, (2010).

[36] J. Froitzheim, H. Ravash, E. Larsson, L.G. Johansson, J.E. Svensson, Investigation of Chromium Volatilization from FeCr Interconnects by a Denuder Technique, J. Electrochem. Soc. 157 (2010) B1295–B1300. doi:10.1149/1.3462987.

[37] C.A. Schneider, W.S. Rasband, K.W. Eliceiri, NIH Image to ImageJ: 25 years of image analysis, Nat Meth. 9 (2012) 671–675. doi:10.1038/nmeth.2089.

[38] S. Molin, M. Chen, P.V. Hendriksen, Oxidation study of coated Crofer 22 APU steel in dry oxygen, Journal of Power Sources. 251 (2014) 488–495. doi:10.1016/j.jpowsour.2013.09.100.

[39] P. Kofstad, High Temperature Corrosion, 1988.

[40] H.L. Lein, T. Tezuka, T. Grande, M.-A. Einarsrud, Asymmetric proton conducting oxide membranes and fuel cells prepared by aqueous tape casting, Solid State Ionics. 179 (2008) 1146–1150. doi:10.1016/j.ssi.2008.01.074.

[41] M. Weirich, J. Gurauskis, V. Gil, K. Wiik, M.-A. Einarsrud, Preparation of lanthanum tungstate membranes by tape casting technique, International Journal of Hydrogen Energy. 37 (2012) 8056–8061. doi:10.1016/j.ijhydene.2011.09.083.

[42] M. Palcut, L. Mikkelsen, K. Neufeld, M. Chen, R. Knibbe, P.V. Hendriksen, Efficient dual layer interconnect coating for high temperature electrochemical devices, International Journal of Hydrogen Energy. 37 (2012) 14501–14510. doi:10.1016/j.ijhydene.2012.07.038.

[43] P. Kofstad, K.P. Lillerud, On High Temperature Oxidation of Chromium II . Properties of and the Oxidation Mechanism of Chromium, J. Electrochem. Soc. 127 (1980) 2410–2419. doi:10.1149/1.2129481.

[44] K. Hoshino, N.L. Peterson, Cation Self-Diffusion in Cr_2O_3, Journal of the American Ceramic Society. 66 (1983) c202–c203. doi:10.1111/j.1151-2916.1983.tb10572.x.

[45] N.J. Magdefrau, L. Chen, E.Y. Sun, M. Aindow, Effects of alloy heat treatment on oxidation kinetics and scale morphology for Crofer 22 APU, Journal of Power Sources. 241 (2013) 756–767. doi:10.1016/j.jpowsour.2013.03.181.

[46] W. Wongpromrat, G. Berthomé, V. Parry, S. Chandra-ambhorn, W. Chandra-ambhorn, C. Pascal, A. Galerie, Y. Wouters, Reduction of chromium volatilisation from stainless steel interconnector of solid oxide electrochemical devices by controlled preoxidation, Corrosion Science. 106 (2016) 172–178. doi:10.1016/j.corsci.2016.02.002.

[47] H. Hindam, D.P. Whittle, Microstructure, adhesion and growth kinetics of protective scales on metals and alloys, Oxid Met. 18 (1982) 245–284. doi:10.1007/BF00656571.

[48] M. Palcut, L. Mikkelsen, K. Neufeld, M. Chen, R. Knibbe, P.V. Hendriksen, Corrosion stability of ferritic stainless steels for solid oxide electrolyser cell interconnects, Corrosion Science. 52 (2010) 3309–3320. doi:10.1016/j.corsci.2010.06.006.

[49] C. Collins, J. Lucas, T.L. Buchanan, M. Kopczyk, A. Kayani, P.E. Gannon, M.C. Deibert, R.J. Smith, D.-S. Choi, V.I. Gorokhovsky, Chromium volatility of coated and uncoated steel interconnects for SOFCs, Surface and Coatings Technology. 201 (2006) 4467–4470. doi:10.1016/j.surfcoat.2006.08.053.

[50] M. Stanislowski, J. Froitzheim, L. Niewolak, W.J. Quadakkers, K. Hilpert, T. Markus, L. Singheiser, Reduction of chromium vaporization from SOFC interconnectors by highly effective coatings, Journal of Power Sources. 164 (2007) 578–589. doi:10.1016/j.jpowsour.2006.08.013.

[51] N.J. Magdefrau, L. Chen, E.Y. Sun, J. Yamanis, M. Aindow, Formation of spinel reaction layers in manganese cobaltite – coated Crofer22 APU for solid oxide fuel cell interconnects, Journal of Power Sources. 227 (2013) 318–326. doi:10.1016/j.jpowsour.2012.07.091.

[52] M. Stanislowski, E. Wessel, K. Hilpert, T. Markus, L. Singheiser, Chromium Vaporization from High-Temperature Alloys I. Chromia-Forming Steels and the Influence of Outer Oxide Layers, J. Electrochem. Soc. 154 (2007) A295–A306. doi:10.1149/1.2434690.

[53] E.J. Opila, N.S. Jacobson, D.L. Myers, E.H. Copland, Predicting oxide stability in high-temperature water vapor, JOM. 58 (2006) 22–28. doi:10.1007/s11837-006-0063-3.

[54] C. Key, J. Eziashi, J. Froitzheim, R. Amendola, R. Smith, P. Gannon, Methods to Quantify Reactive Chromium Vaporization from Solid Oxide Fuel Cell Interconnects, Journal of The Electrochemical Society. 161 (2014) C373–C381.

[55] J. Issartel, S. Martoia, F. Charlot, V. Parry, G. Parry, R. Estevez, Y. Wouters, High temperature behavior of the metal/oxide interface of ferritic stainless steels, Corrosion Science. 59 (2012) 148–156. doi:10.1016/j.corsci.2012.02.025.

[56] P. Huczkowski, N. Christiansen, V. Shemet, L. Niewolak, J. Piron-Abellan, L. Singheiser, W.J. Quadakkers, Growth Mechanisms and Electrical Conductivity of Oxide Scales on Ferritic Steels Proposed as Interconnect Materials for SOFC's, Fuel Cells. 6 (2006) 93–99. doi:10.1002/fuce.200500110.

[57] L. Mikkelsen, M. Chen, P.V. Hendriksen, Å. Persson, N. Pryds, K. Rodrigo, Deposition of $La_{0.8}Sr_{0.2}Cr_{0.97}V_{0.03}O_3$ and $MnCr_2O_4$ thin films on ferritic alloy for solid oxide fuel cell

application, Surface and Coatings Technology. 202 (2007) 1262–1266. doi:10.1016/j.surfcoat.2007.07.046.

[58] I.-H. Jung, Critical evaluation and thermodynamic modeling of the Mn–Cr–O system for the oxidation of SOFC interconnect, Solid State Ionics. 177 (2006) 765–777. doi:10.1016/j.ssi.2006.01.012.

[59] M.G.C. Cox, B. McEnaney, V.D. Scott, Kinetics of initial oxide growth on Fe-Cr alloys and the role of vacancies in film breakdown, Philos Mag. 31 (1975) 331–338.

[60] R.E. Lobnig, H.P. Schmidt, K. Hennesen, H.J. Grabke, Diffusion of cations in chromia layers grown on iron-base alloys, Oxidation of Metals. 37 (1992) 81–93.

[61] E. Aukrust, A. Muan, Phase Relations in the System Cobalt Oxide–Manganese Oxide in Air, Journal of the American Ceramic Society. 46 (1963) 511–511. doi:10.1111/j.1151-2916.1963.tb13790.x.

[62] W.J. Quadakkers, K. Bongartz, The prediction of breakaway oxidation for alumina forming ODS alloys using oxidation diagrams, Materials and Corrosion. 45 (1994) 232–241. doi:10.1002/maco.19940450404.

[63] X. Montero, N. Jordán, J. Pirón-Abellán, F. Tietz, D. Stöver, M. Cassir, I. Villarreal, Spinel and Perovskite Protection Layers Between Crofer22APU and $La_{0.8}Sr_{0.2}FeO_3$ Cathode Materials for SOFC Interconnects, J. Electrochem. Soc. 156 (2009) B188–B196. doi:10.1149/1.3025914.

[64] L. Blum, U. Packbier, I.C. Vinke, L.G.J. de Haart, Long-Term Testing of SOFC Stacks at Forschungszentrum Jülich, Fuel Cells. 13 (2013) 646–653. doi:10.1002/fuce.201200151.

[65] S. Taniguchi, M. Kadowaki, H. Kawamura, T. Yasuo, Y. Akiyama, Y. Miyake, T. Saitoh, Degradation phenomena in the cathode of a solid oxide fuel cell with an alloy separator, Journal of Power Sources. 55 (1995) 73–79. doi:10.1016/0378-7753(94)02172-Y.

[66] E. Konysheva, H. Penkalla, E. Wessel, J. Mertens, U. Seeling, L. Singheiser, K. Hilpert, Chromium Poisoning of Perovskite Cathodes by the ODS Alloy Cr5Fe1Y2O3 and the High Chromium Ferritic Steel Crofer22APU, J. Electrochem. Soc. 153 (2006) A765–A773. doi:10.1149/1.2172563.